

Transfer doping of Graphene by Species of Extreme Work Function

Haichang Lu¹, Yuzheng Guo², John Robertson^{1*}

¹Department of Engineering, Cambridge University, Cambridge CB3 0FA, United Kingdom

²College of Engineering, Swansea University, Swansea SA1 8EN, United Kingdom

E-mail: jr214@cam.ac.uk

Keywords: Graphene, transfer doping, conductivity, electronic devices.

Abstract: Density functional calculations are used to explain the charge transfer doping mechanism by which species physisorptively bonded to graphene can increase its free hole or electron density, without giving rise to defects, and thus maintain a high carrier mobility. Typical dopants studied are FeCl₃, AuCl₃, SbF₅, HNO₃, MoO₃, Cs₂O and O₂. These systems do not break the π bonding of the basal plane are particularly important as these do not degrade the carrier mobility. In contrast, more reactive radicals like -OH cause a puckering of the basal plane and thereby act as defects.

Introduction

Graphene is a two-dimensional material with a unique band structure with bands crossing at the Dirac point.¹ This gives graphene a very high carrier mobility, but the carrier concentration is small, so that its overall electrical conductivity is rather low.² Thus graphene must be doped to increase carrier concentration in order to realize some of its main applications such as a transparent electrode in displays or photovoltaic devices.²⁻⁶ Doping is also useful to increase the sensitivity of graphene when used as a molecular sensor.⁷⁻¹⁰

The conventional way to dope a 3-dimensionally bonded semiconductor would be by substitutional doping. This has indeed been carried out for graphene using nitrogen or boron doping.⁹⁻¹¹ Substitutional sites have the advantage that they are fully bonded into the lattice and are thus stable. However, nitrogen can enter the graphene lattice in various configurations, only one of which is the actual doping configuration.^{12,13} The other configurations not only do not dope, they also introduce defects^{14,15} which cause carrier scattering and so they degrade the carrier mobility. This ‘functionalization’ is useful in other contexts such as creating catalytic sites in carbon nanotubes.¹⁴ On the other hand, for graphene as an electrode, it is useful to consider interstitial or transfer doping by physisorbed species.¹⁶⁻²³ These can dope the graphene n-type or p-type, without necessarily creating defects. Transfer doping is also useful to increase

the conductivity of contacts, as the high resistance of contacts to graphene in devices can limit the device performance.

We consider the cases of very electronegative and electropositive species, (strong Lewis acids and Lewis bases). These cases are often related to previously studied cases of the intercalation of graphite,^{24,25} or the transfer doping of organic molecules for example for organic light emitting diodes.^{26,27} We also consider radical species with empty states below the graphene Fermi energy. The second factor of interest is whether the dopant species disturbs the π bonding of the basal plane and thus introduces sp^3 sites in the otherwise sp^2 bonding. This leads to a loss of carrier mobility.

Methods

The calculations are carried out using periodic supercell models of the graphene and the dopant species using the CASTEP plane-wave density functional theory (DFT) code, with ultra-soft pseudopotentials and the Perdew-Burke-Ernzerhof (PBE) form of the generalized gradient approximation (GGA) for the electronic exchange-correlation functional. For the open shell magnetic system $FeCl_3$, we use the GGA+U method, with an on-site potential U of 7 eV applied to the Fe 3d states.

The dispersion correction to the GGA treatment of the van der Waals interaction is included using the Tkatchenko-Scheffler (TS) scheme. To overcome the error induced by periodical mirror charge, self-consistent dipole correction is implemented. The plane wave cut-off energy is 380eV, as the cut-off energy of oxygen.

For the graphene plus dopant system, a layer-by-layer stacked supercell is created in each case, with a close degree of lattice matching between the graphene and the dopant. A 30Å vacuum layer is included where a vacuum layer is needed. The size of the supercell is given in Table. 1. A dense 9×9 k-point mesh is used, as graphene needs a dense k-point due to its small density of

states close to the Dirac point. The calculated lattice constant of graphene in PBE is 2.47Å, 0.4% less than the experimental value.¹

Doping causes a shift in the system's Fermi energy away from the Dirac point of the graphene. This shift is compared to the Fermi energy, ionization potential or electron affinity of the isolated dopant system. These energies are calculated using a periodic supercell of the dopant species plus vacuum gap. The electrostatic potential is calculated for the dopant system layers, averaged along the layers. The potential in the vacuum gap region gives the vacuum potential. The energy of the valence band maximum is then compared to the vacuum energy to give the ionization potential, and with the band gap, the electron affinity.

Results

We first consider Lewis acids such as $AuCl_3$. Crystalline $AuCl_3$ consists of stacked layers of Au_2Cl_6 molecular units. The Au_2Cl_6 molecule consists of two planar edge-connected $AuCl_4$ squares. The supercell consists of alternate graphene and $AuCl_3$ layers along the z axis. Fig. 2(a) shows the 4x4 graphene supercell with the planar Au_2Cl_6 units separated from each other in-plane at a similar distance as in pure $AuCl_3$. The position of Au_2Cl_6 units on the graphene is allowed to vary to minimize the total energy.

Fig. 2(c) shows the band structure of isolated pure Au_2Cl_6 in the hexagonal lattice. The Au_2Cl_6 is a semiconductor with a band gap of 1.22 eV. The Au 5d band is filled to $d^{9.6}$. The conduction band consists of the Au s state and Cl p states. Fig. 2(d) shows the band structure of the combined system. As a 4x4 supercell was used, the graphene Dirac point still lies at K, and can

be recognized as the crossed bands at 1.02 eV. This shows that the shift of the Fermi energy E_F due to this AuCl_3 doping concentration is 1.02 eV.

Fig. 2(b) shows these results in a density of states (DOS) plot. The doping has occurred by a transfer of electrons from its valence band into the AuCl_3 conduction band filling its conduction bands lying just below 0 eV in the central panel of Fig. 2(b).

We next consider FeCl_3 , which is another Lewis acid like AuCl_3 . It has been extensively used as an intercalant of graphite, as discussed by Li *et al.*³⁷ Solid FeCl_3 forms a layered system of Fe_2Cl_6 edge-connected octahedra connected along three directions at 120° to each other. The Cl sites are rotated slightly off the vertical. The hexagonal supercells of graphene and FeCl_3 can be made with a 23\AA periodicity. On the other hand, we achieve a smaller $\sqrt{7}\times\sqrt{7}$ supercell using a 1×1 periodicity of the FeCl_3 sublattice and a $\sqrt{7}\times\sqrt{7}$ periodicity of the graphene, as in Fig. 3(a). FeCl_3 is a magnetic semiconductor with a 0.7 eV band gap. A vertical stacking of one FeCl_3 layer and one graphene layer along Oz is ferromagnetic. A stacking of two FeCl_3 layers and two graphene layers along Oz as here allows the FeCl_3 to be anti-ferromagnetically (AF) ordered, which simplifies the band structure plots (the spin-up and spin-down bands are degenerate). Fig. 3(c) shows the AF bands of isolated FeCl_3 calculated for a value of $U=7$ eV, with the 0.7 eV band gap. The Fe 3d occupancy is $d^{5.6}$.

Fig. 3(d) shows the band structure of the combined system. The graphene Dirac point can be recognized at the K point 1.0 eV above the Fermi energy. Fig. 3(b) shows the density of states for the combined system and for the isolated FeCl_3 . Doping has occurred by transfer of electrons from the upper graphene valence band to the FeCl_3 conduction states at -0.1 eV in Fig. 3(b).

We then consider the strongest Lewis acid SbF_5 . Condensed SbF_5 can be considered to form a network of corner-sharing octahedral with the F sites vertically above each other. The SbF_5 units form chains which are conveniently lattice-matched to graphene, when a supercell of 1×1 SbF_5 and $\sqrt{3}\times\sqrt{3}$ is used, as in Fig. 4(a).

Fig. 4(c) shows the band structure of isolated SbF_5 in the unit cell of Fig. 4(a). It is a semiconductor with a GGA band gap of 3.06 eV, and a direct gap at Γ . This system contains only s,p electrons and Sb is in its +5 valence state. The top of the valence band consists of F $2p\pi$ states the conduction band minimum consists of empty Sb 5s states.

Fig. 4(d) shows the band structure of the combined system. Due to the orientation of the graphene and SbF_5 sub lattices, the Dirac point folds over to appear at Γ , at about 1.0 eV above the combined Fermi energy. Fig. 4(b) shows the density of states of the combined systems, and the isolated graphene. Doping has occurred by transfer of electrons from the graphene valence band into SbF_5 conduction band. This has caused a 3.00 eV shift of the SbF_5 bands, but only a 1.05 eV downward shift of the E_F of graphene.

Table. 3 gives the calculated electron affinity, band gap and ionization potential of these compounds. As ideal isolated semiconductors, their Fermi energies would appear near midgap. In practice, the anion vacancy is the lowest energy defect in these systems, and this defect is calculated to be shallow. Thus, in practice their Fermi energy is likely to lie close to their conduction band edges. The large electronegativity of the halogens means that the valence bands of these systems are very deep below the vacuum level. Even with E_F lying at their conduction band edges, their work functions are still very large, much larger than that of the most electropositive metal, Pt.

We now pass to the case of MoO_3 . This oxide has been widely used as a p-type dopant and electrode material in organic electronics, and has recently been used for p-type doping in carbon nanotubes, graphene and MoS_2 contacts. MoO_3 has two forms, the molecule Mo_3O_9 , and a

layered solid form MoO₃. MoO₃ was previously calculated to have a band gap of 3.0 eV and an electron affinity of 6.61 eV. Its oxygen vacancies were calculated to be shallow. The doping of MoS₂ and carbon nanotubes by MoO₃ layers has already been studied theoretically.

An orthorhombic supercell of graphene and MoO₃ was constructed as in Fig. 5(a). The electronic structure of the combined system was calculated. The large work function of MoO₃, 6.60 eV below that of graphene, means that there is a strong transfer doping. It is found that the Fermi energy of the combined system has shifted downwards in the graphene by 0.63 eV. In this case, doping has occurred by the transfer of electrons from the graphene valence band to the MoO₃ conduction band states. Nevertheless, the bonds between graphene and the outer O layer of MoO₃ are only physisorptive with a bond length of 2.5 Å. The MoO₃ does not cause any puckering of the graphene sp² sites and thus does not affect the π bonding of the graphene layer. Thus, the C atoms do not act as defects under this doping process. There will be no Raman D peak, and no carrier scattering. This is consistent with experiment where singularly Chen *et al.*¹⁶ find that MoO₃ doped graphene retains the ability to show a quantum Hall effect, indicating a high carrier mobility.

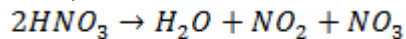
MoO₃ is a very valuable dopant of graphene because it is a stable dopant, it raises the carrier concentration, it does not degrade the carrier mobility by causing defects, it has a wide band gap so that it is also optically transparent, a very useful combination useful for optical devices.

We now consider an n-type transfer dopant, CsO_x. Cs carbonate is widely used as an n-type dopant in organic light emitting diodes, and also can be used to dope graphene. The carbonate precursor dissociates on heating to leave a Cs oxide, which may actually be a sub-oxide. We consider the oxide to be Cs₂O. This has the inverse CdCl₂ hexagonal layered structure, with the Cs layers on the outside and O atoms on the inside. Note that whereas the interlayer bonding in CdCl₂ is van der Waals, the Cs-Cs bonding in Cs₂O is essentially metallic, not van der Waals. The hexagonal layers are reasonably lattice-matched to those of graphene, with a 1.6% mismatch, as shown in Table. 1 and Fig. 6(a). The Cs and O sites lie over the hollow sites of the graphene lattice.

Fig. 6(c) and (d) shows the band structure of isolated Cs₂O. Cs₂O is a semiconductor with a band gap of 1.44 eV in screened exchange and a very low electron affinity. Its valence band consists of oxygen 2p states. The valence band is very narrow because the O sites are far apart, so the O-O interface controlling the VB width is weak.

Fig. 6(e) shows the density of states for the combined system. There is strong n-type doping, with electrons transferred from the Cs₂O valence band into the graphene conduction band. The E_F of graphene is shifted upwards by 0.95 eV by the Cs₂O layer. Nevertheless the Cs-C bond is long and physisorptive. It is not van der Waals, and no van der Waals correction to GGA is used in this case. The graphene atoms remain unpuckered below the Cs₂O and sp² bonding is maintained in the graphene. This behavior is consistent with the behavior of Cs₂O as an n-type transfer dopant in organic semiconductors.^{17,18}

Nitric acid is another p-type dopant, but it functions differently. Nistor *et al.*³² studied the absorption of HNO₃ onto the graphene surface. They found that HNO₃ dissociates into an NO₃ radical, a NO₂ radical and a water molecule,



HNO₃ is introduced into the 5x5 supercell. Dissociation occurs. These species are allowed to rotate to maximize their stability. The final geometry is shown in Fig. 7(a). The NO₃ radical lies planar parallel to the graphene plane, with each of its atoms lying on top of a carbon atom. The

NO₂ radical and the water molecule lie in a plane normal to the graphene plane, with the central N atom of NO₂ and central O atom of H₂O nose down towards the graphene, as in Fig. 7(b). These species are physisorbed onto the graphene, and the bond lengths are given in Table. 2. None of the species cause any buckling of the underlying graphene layer. The binding energy (Table. 2) is relatively small.

Whereas H₂O is a closed shell system, both NO₃ and NO₂ are radicals each with a half-filled orbital. Critically, the work function of this orbital is greater than that of the graphene, the state lies deeper below the vacuum level than the Fermi energy E_F of graphene. Thus, they give a singly empty state lying below E_F . This leads to an electron transfer from the graphene into the two NO_x species, filling their states, and thus causing a hole doping of the graphene. As the bond length is long, there is only partial charge transfer. The charge transfer is calculated to be -0.3e on the NO₃ and -0.25e on the NO₂. This lowers E_F of the graphene to -1.10 eV, as shown in Fig. 7(c). The retention of planar sp² bonding in the C sites under the NO₃ and NO₂ physisorbed species means that this does not constitute a defect, there is no Raman D peak and no carrier scattering. This is consistent with experiment. L'Arsie finds no change in the D peak intensity experimentally.¹⁹

We now consider Cl₂. Cl₂ is a closed shell molecule with a single Cl-Cl bond. It has a filled p σ state at -12 eV, two filled p π states and two filled p π^* states, followed by an empty σ^* state above its Fermi energy. The Cl₂ molecule is physisorbed onto graphene, but it does not produce doping because it has no empty states below E_F of graphene (Fig. 8). There is no doping because the empty σ^* state is high in energy despite the electronegativity of Cl.

Following Cl₂, we consider the O₂ molecule. This molecule is calculated to physisorb in a configuration across a C-C bond, as in Fig. 9(a). Now, the O₂ molecule is geometrically the same as the Cl₂ molecule, but its π^* states would be half-filled in the spin unpolarized condition. This configuration is unstable to against symmetry breaking to open up a band gap. This occurs by an antiferromagnetic ordering of the σ^* spins, with the up-spin states lying below E_F and the down-spins lying above the gap. For the combined O₂ on graphene system, the gap is small enough that the empty spin-down σ^* state lie below E_F of isolated graphene, so there is a sizable charge transfer doping of the graphene by O₂, as shown in Fig. 9(b).

Finally, we consider the -OH radical. The O-H bond creates a deep-lying filled σ state, and a high-lying empty σ^* state. The other broken O bond makes the unpaired electron of the radical. As O is very electronegative, this p state lies well below E_F of isolated graphene. More interesting, this p state is able to form a strong C-O bond to a carbon atom underneath, puckering the C atom out of the plane, and converting it into a sp³ configuration (Fig. 10). Thus, there is charge transfer from the graphene. However the overall effect on conductivity will be poor because the defect states will lower the mobility.

Overall, except for OH, there various dopants studied are physisorbed, without puckering the underlying graphene. This occurs because of the strong intra-layer rigidity of graphene, and its resistance to out-of-plane deformation needed to form the fourth extra bond to a chemisorbing species. We now show that this also applies to transfer dopants on hydrogen terminated diamond surfaces.

Discussion.

The electron affinity and ionization potentials of the various dopant species can be calculated using dopant supercells as described in the Methods section. The Fermi level shifts (FLS) are

compared with the ionization potentials (IP) in Table. 1. We see that there is monotonic variation of the FLS with the IPs. The largest p-type shift occurs for SbF_5 and FeCl_3 has the largest shift of the more common dopants FeCl_3 , AuCl_3 , and HNO_3 .

The SbF_5 , FeCl_3 and AuCl_3 species have remarkably large ionization potentials, if the band gaps are added to the work functions.

Experimentally, FeCl_3 is found to give the largest E_F shift of the common dopants FeCl_3 , AuCl_3 , MoO_3 and HNO_3 .^{33,34} Also, the absence of a Raman D peak at 1350 cm^{-1} confirms that FeCl_3 , MoO_3 and HNO_3 do not give rise to basal plane defects,^{17,19,33} and thus should not increase carrier scattering. Our calculations have a similar aim as those of Hu and Gerber.³¹ For FeCl_3 , our calculations are for the spin-polarized state using GGA+U whereas Liu *et al.*³⁵ used spin unpolarized state. We used a three times smaller supercell than in Zhan *et al.*³³ by rotating the x,y axes. For HNO_3 doping we found that the acid dissociates, as in Nistor *et al.*³²

Conclusions

We have calculated the conditions required for charge transfer doping of graphene (sometimes called non-covalent doping). We find that the Fermi level shift in eV is proportional to the electron affinity of the acceptor species or ionization potential of the donor species. We have treated a wider range of dopant species than other groups. The doping mechanism is similar to that occurring in transfer doping of organic semiconductors. We thank EPSRC grant EP/P005152/1 and CSC for support.

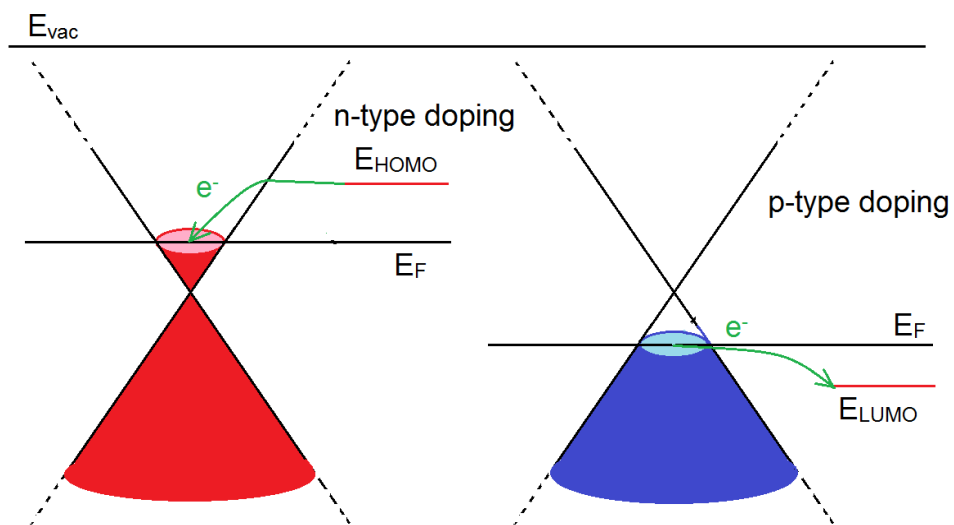


Figure 1. Schematic of n-type and p-type doping process in Graphene.

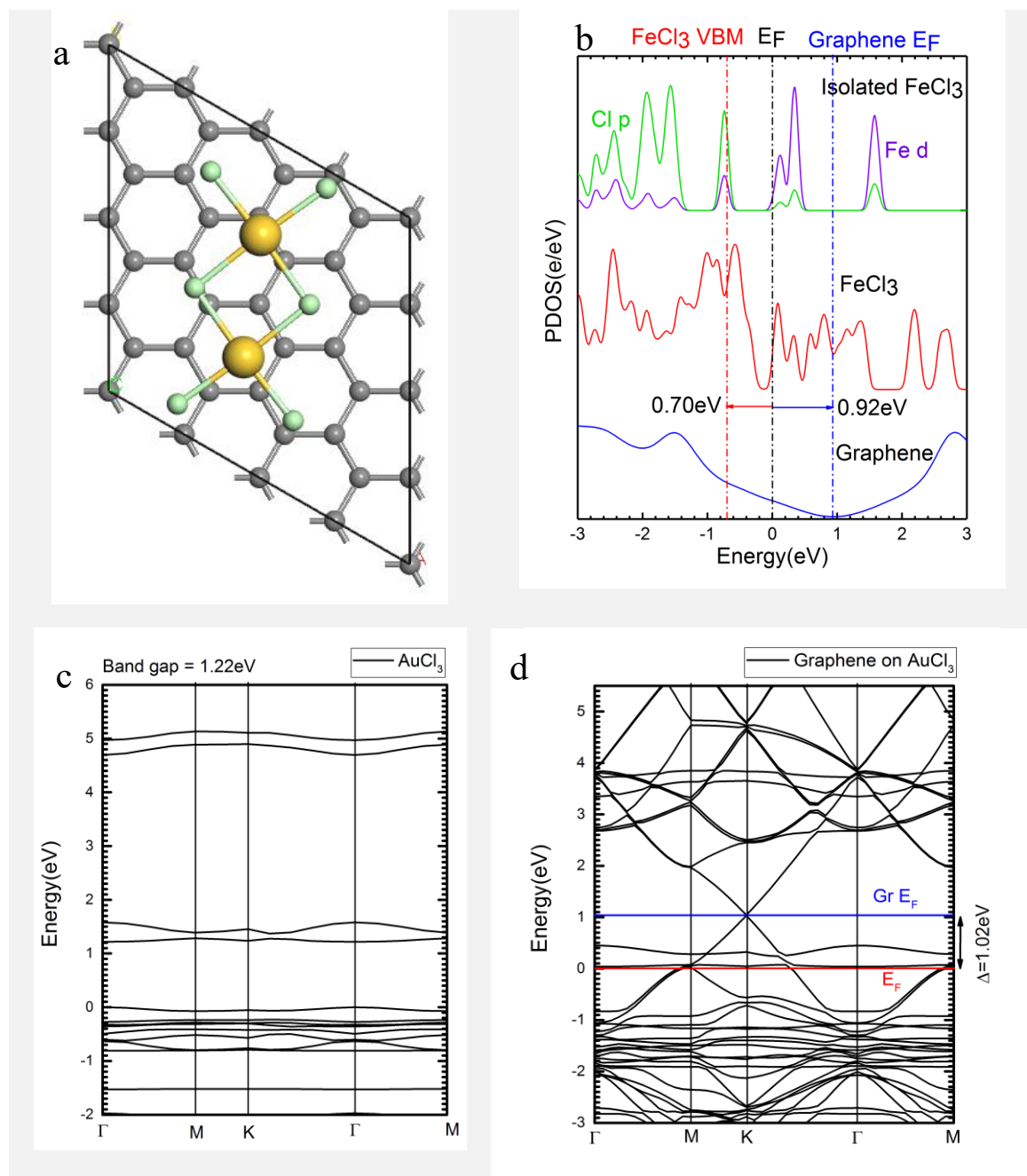


Figure 2. (a) Au₂Cl₆ molecular on 4x4 Graphene supercell. (b) PDOS of isolated AuCl₃ and AuCl₃/Graphene system. (c) Band Structure of isolated pure Au₂Cl₆ in the hexagonal lattice. (d) Band Structure of the combined system.

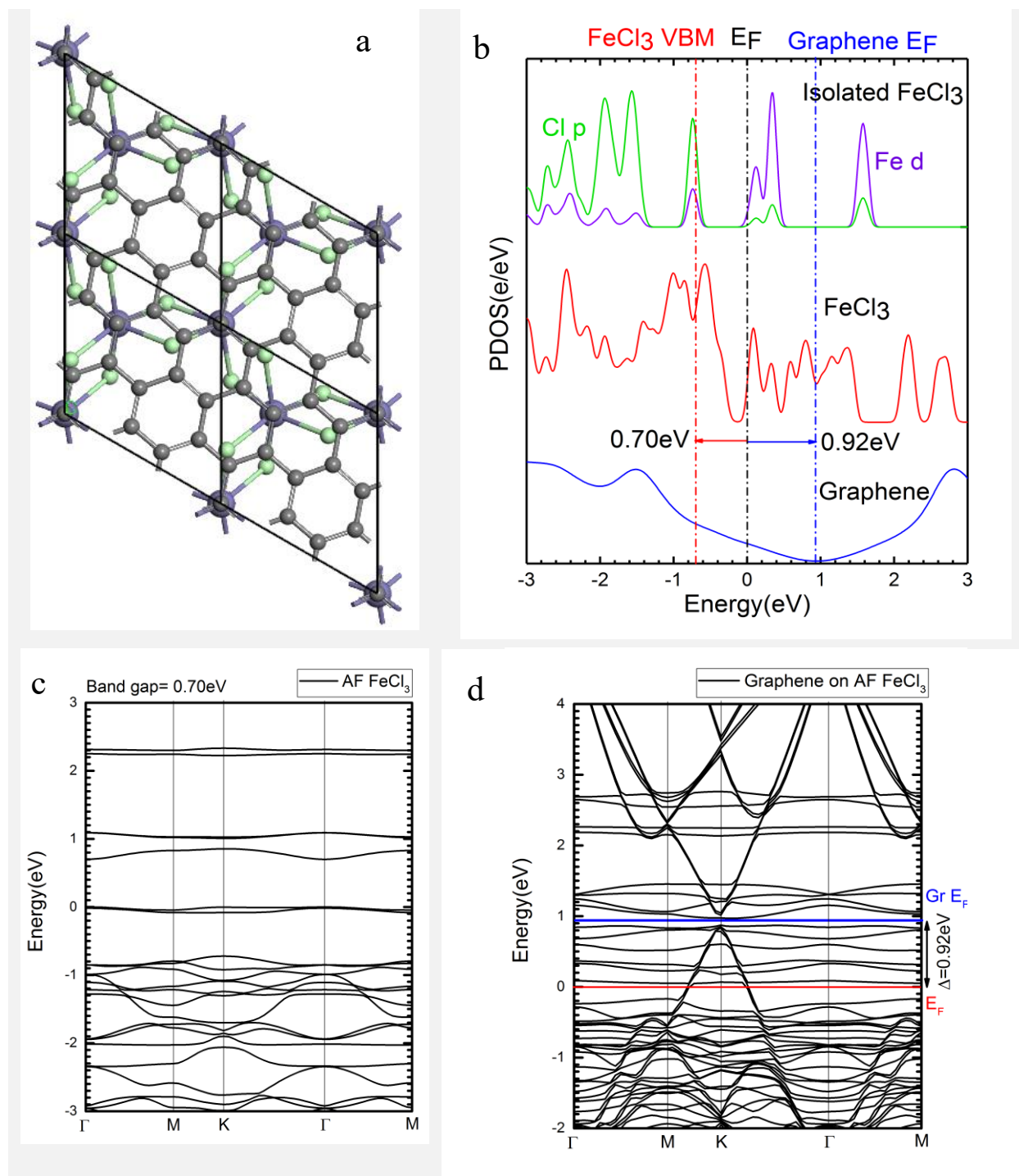


Figure 3. (a) FeCl₃ on $\sqrt{7} \times \sqrt{7}$ Graphene supercell. (b) PDOS of isolated AF FeCl₃ and FeCl₃/Graphene system. (c) Band Structure of isolated pure AF FeCl₃. (d) Band Structure of the combined system.

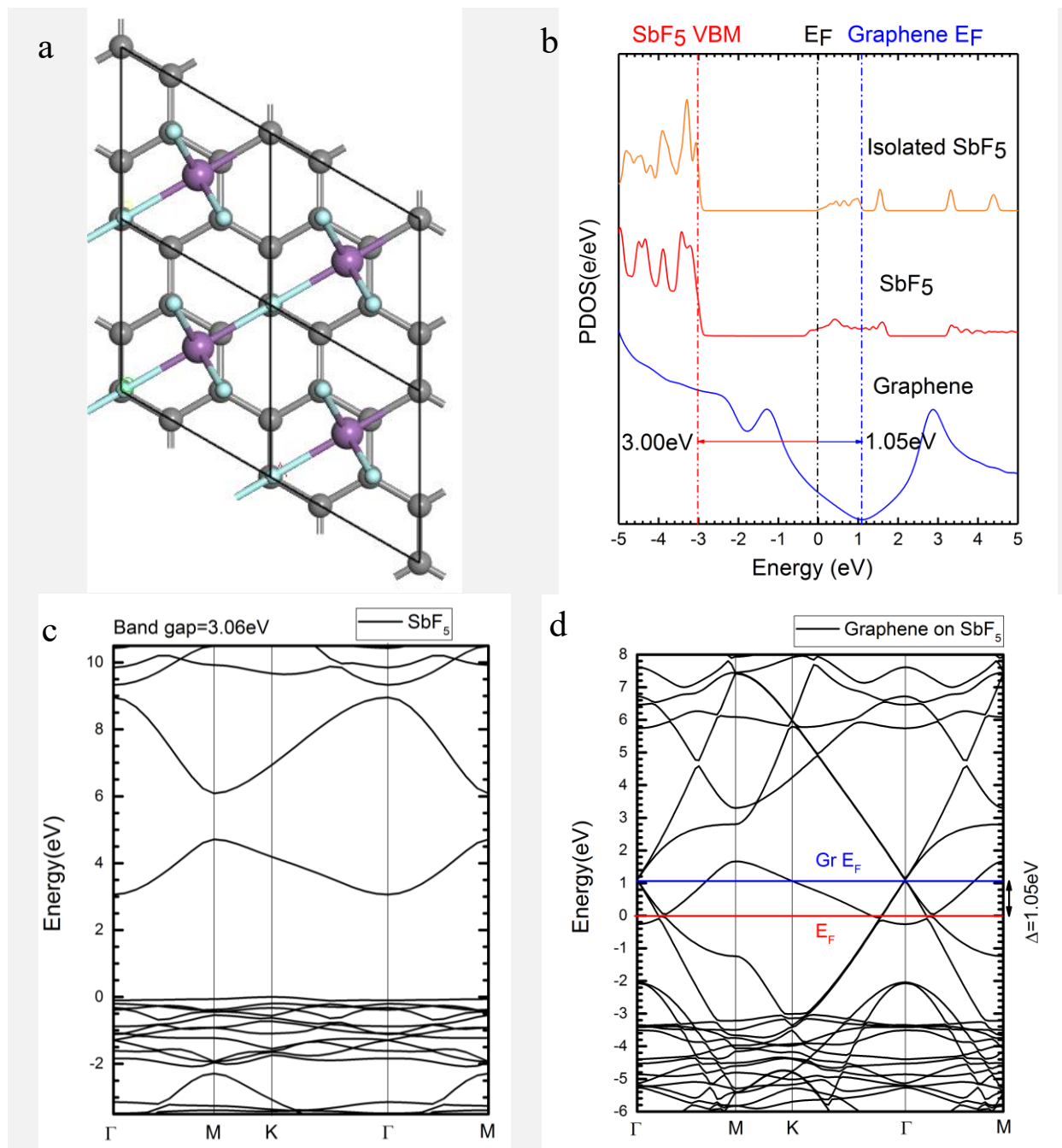


Figure 4. (a) SbF₅ on $\sqrt{3} \times \sqrt{3}$ Graphene supercell. (b) PDOS of isolated SbF₅ and SbF₅/Graphene system. (c) Band Structure of isolated pure SbF₅ single layer in the hexagonal lattice. (d) Band Structure of the combined system.

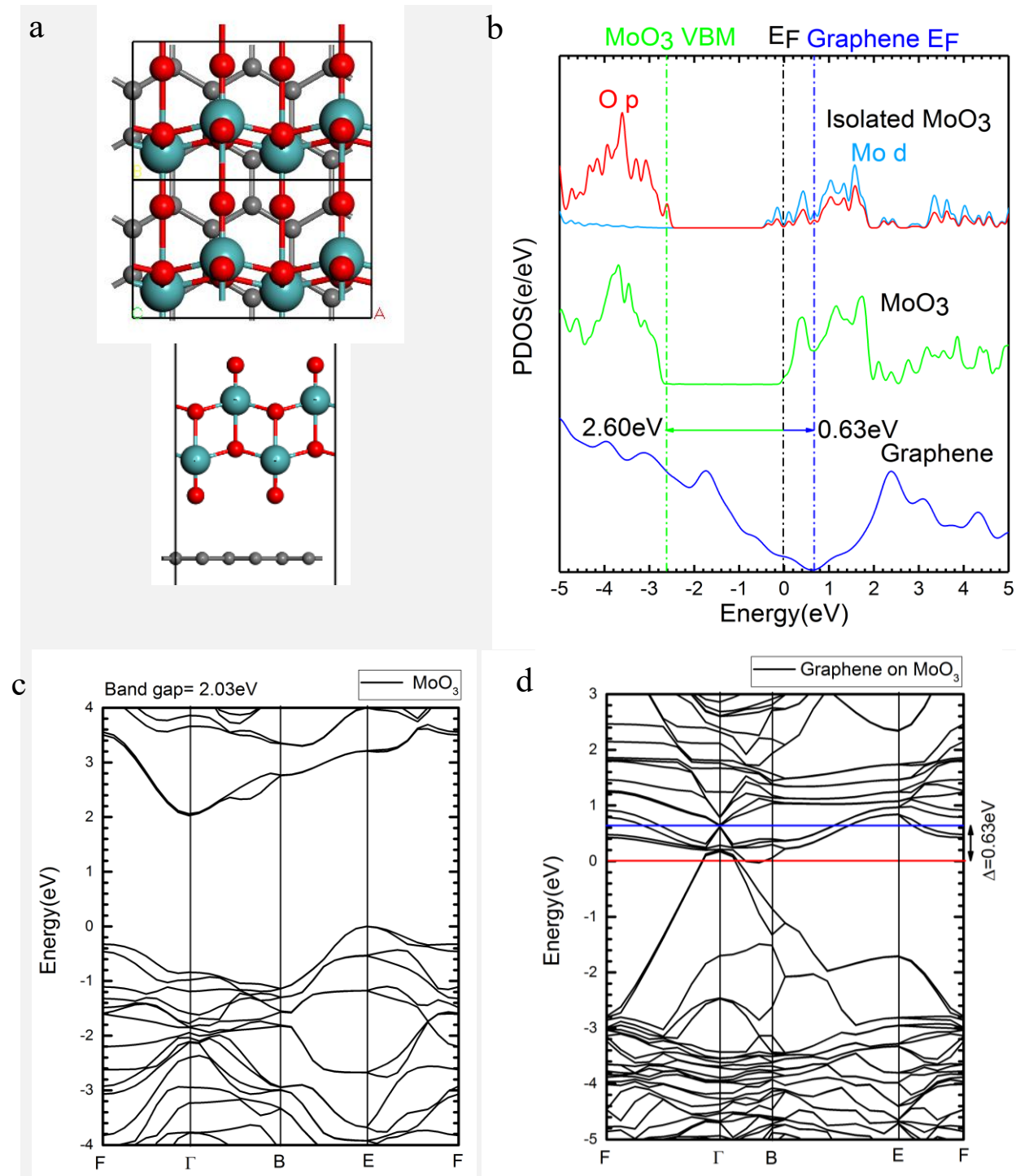


Figure 5. (a) MoO₃ on 3x√3 Graphene supercell. (b) PDOS of isolated MoO₃ and MoO₃/Graphene system. (c) Band Structure of isolated pure single layer MoO₃. (d) Band Structure of the combined system.

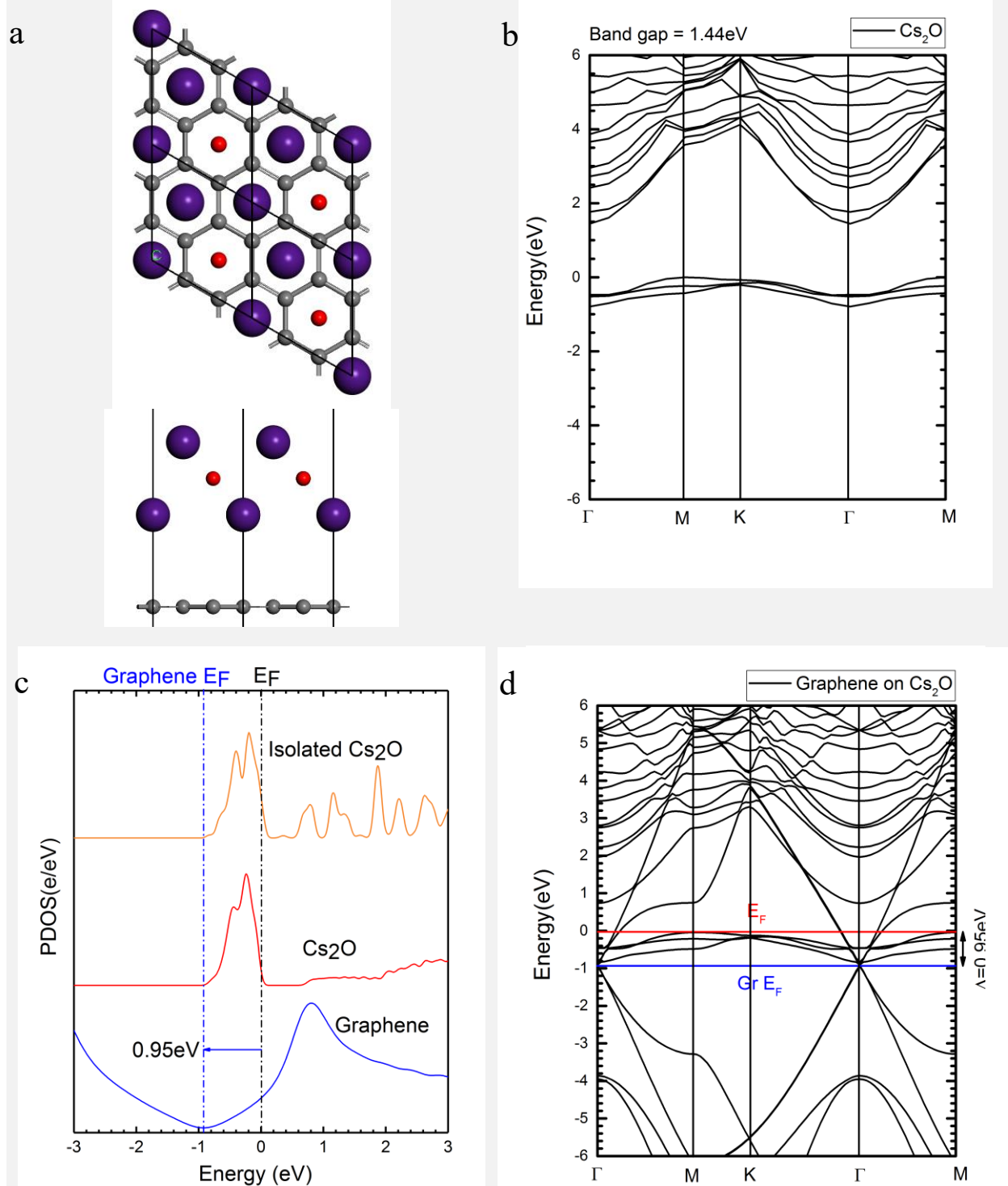


Figure 6. (a) Top view and (b) side view of Cs₂O on $\sqrt{3}\times\sqrt{3}$ Graphene supercell. (c) GGA and (d) screened exchange Band Structure of isolated pure single layer Cs₂O. (e) PDOS of isolated Cs₂O and Cs₂O/Graphene system. (f) Band Structure of the combined system.

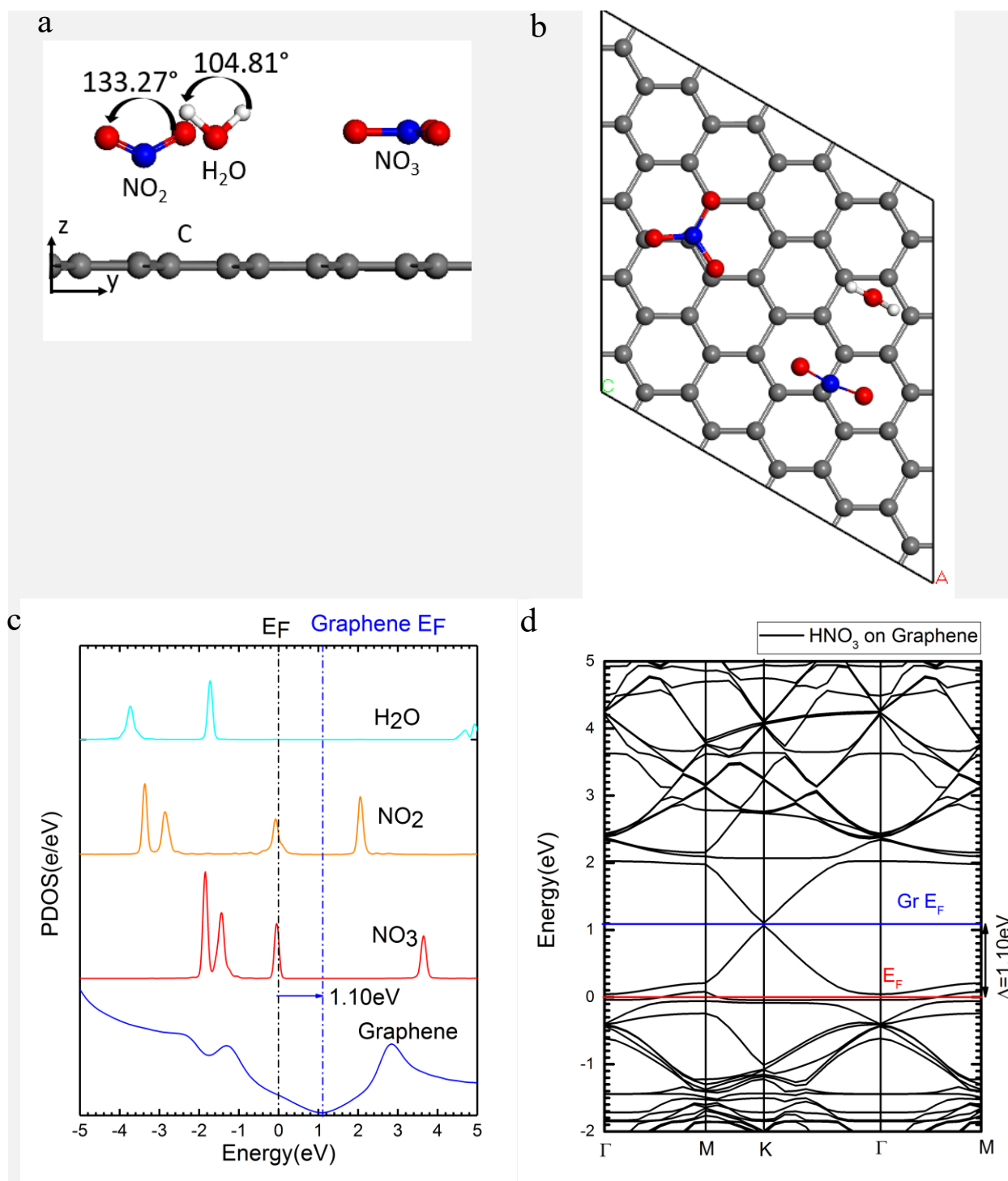


Figure 7. (a) Side view and (b) top view of 2HNO₃ dissolve onto 5x5 Graphene supercell. (c) PDOS of 2HNO₃/Graphene system. (d) Band Structure of the combined system.

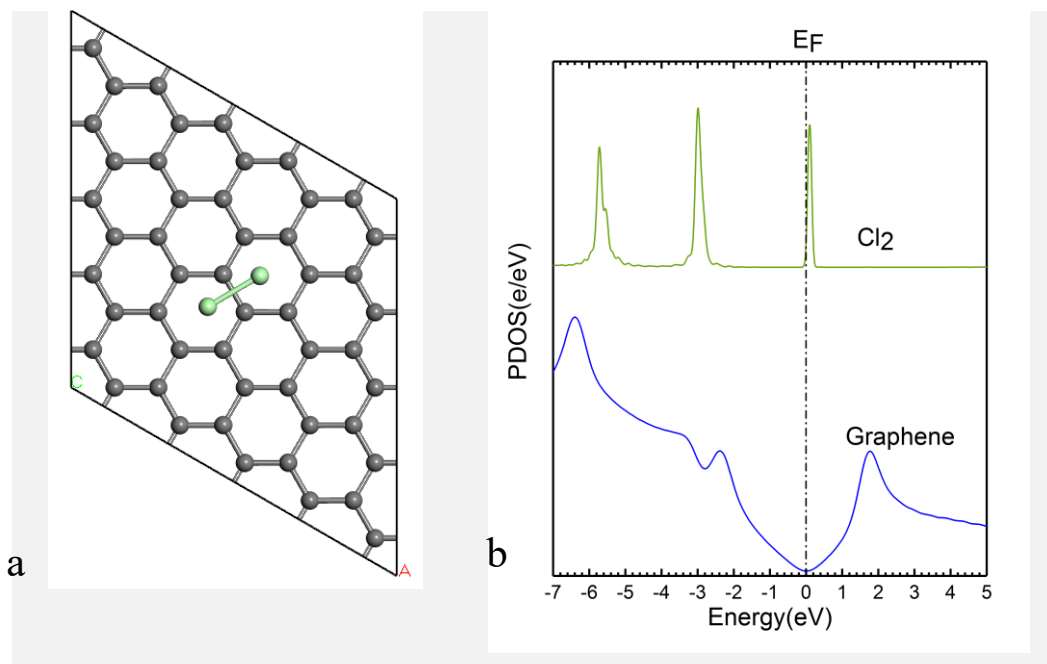


Figure 8. (a) Top view of Cl_2 on 5×5 Graphene supercell. (b) PDOS of $\text{Cl}_2/\text{Graphene}$ system.

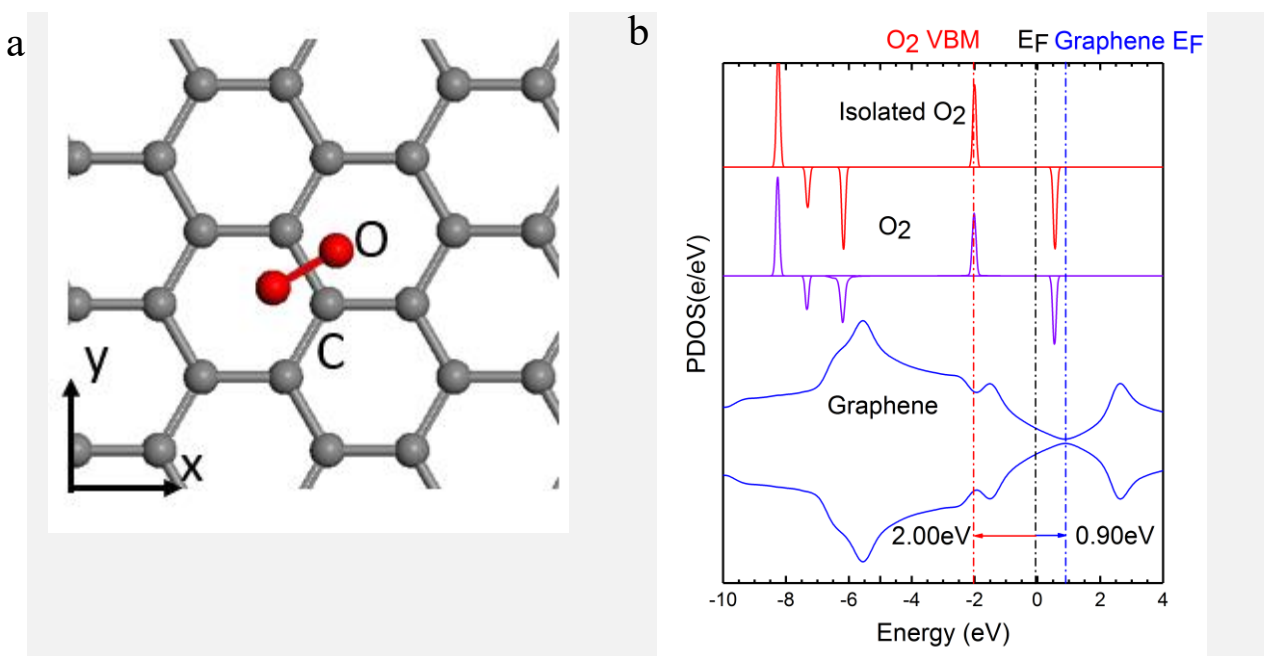


Figure 9. (a) Top view of triplet O_2 on 5×5 Graphene supercell. (b) PDOS of $\text{O}_2/\text{Graphene}$ system.

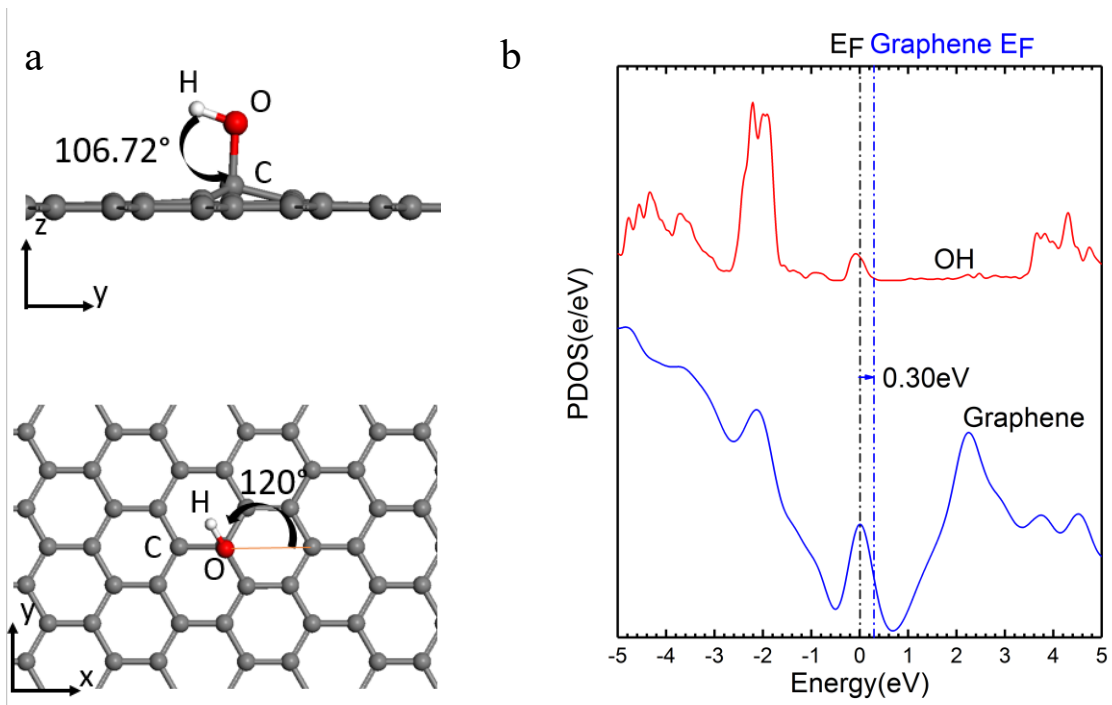


Figure 10. (a) Side view and (b) top view of OH radical bonding onto 5x5 Graphene supercell.
 (c) PDOS of OH/Graphene system.

Table 1. Supercell and lattice match of Graphene and dopant. M in the mismatch column refers to a molecular dopant where there is no mismatch.

	Graphene supercell/ Dopant supercell	Mismatch rate (%)
SbF₅	$\sqrt{3} \times \sqrt{3}/1 \times 1$	1.66
FeCl₃	$\sqrt{7} \times \sqrt{7}/1 \times 1$	1.42
AuCl₃	$4 \times 4/1 \times 1$	M
MoO₃	$3 \times \sqrt{3}/2 \times 1$	0.34, 7.92
Cs₂O	$\sqrt{3} \times \sqrt{3}/1 \times 1$	1.62
Cl₂	5×5	M
O₂	5×5	M
OH	5×5	M
HNO₃	5×5	M

Table 2. Atomic distance, bond length and puckering of Graphene.

	Bond type	Bond (Å)	Surface distance (Å)	Puckering (Å)	Binding energy (eV)
OH	O-H	0.98	—	0.51	-1.64
	C-O	1.51	—		
O₂	O-O(in O ₂)	1.24	3.29	0.09	-0.13
HNO₃	O-H(in H ₂ O)	0.98	3.28	0.06	-0.39
	N-O(in NO ₂)	1.23	2.60		
	N-O(in NO ₃)	1.27	3.25		

Table 3. Atomic distance, bond length and puckering of Graphene. Layer distance, work function, ionization potential and Fermi level shift.

	Layer distance (Å)	Work Function (eV)	Ionization potential (eV)	FLS (eV)
SbF₅	3.65	7.04	-	-1.05
FeCl₃	3.54	6.97	-	-0.92
MoO₃	2.95	6.61	-	-0.63
AuCl₃	3.35	5.94	-	-1.02
Cs₂O	3.75	-	2.35	0.95

REFERENCES

1. Geim, A.K.; Novoselov, K. S. The rise of graphene, *Nature Mater.* **2007**, 6, 183-191.
2. De, S.; Coleman, J. N. Are there fundamental limits on sheet resistance and transmittance of thin graphene films? *ACS Nano*, **2010**, 4, 2713-2720.
3. Bae, S.; Kim, H.; Lee Y. et al. Roll-to-roll production of 30-inch graphene films for transparent electrodes, *Nature Nanotech.* **2010**, 5, 574-578.
4. Zhong, G.; Wu, X.; D'Arsie L. et al. Growth of continuous graphene by open roll-to-roll chemical vapor deposition. *Appl. Phys. Lett.* **2016**, 109, 193103.
5. Sato, S.; Graphene for Nano-electronics. *Jpn. J. App. Phys.* **2015**, 54, 040102.
6. Hofmann, S.; Brauninger-Weimer, P.; Weatherup, R. S. CVD enabled graphene manufacture and technology, *J. Phys. Chem. Lett.* **2015**, 6, 2714-2721.
7. Schedin, F.; Geim, A. K.; Morozov, S. V.; Hill, E.W.; Blake, P.; Katsnelson, M. I.; Novoselov, K. S. Detection of individual gas molecules adsorbed on graphene, *Nature Mater.* **2007**, 6, 652-655.
8. Wehling, T. O.; Novoselov, K. S.; Morozov, S. V.; Vdovin, E. E.; Katsnelson, M. I.; Geim, A. K. Molecular doping of graphene, *Nano Lett.* **2008** 8, 173-177.
9. Lv, R. T.; Chen, G. G.; Li, Q.; McCreary, A.; Botello-Mendez, A.; Morozov, S. V.; Liang, L. B.; Declerk, X.; Perea-Lopez, N.; Culleni, D. A.; Novoselov, K. S.; Terrones, M. Ultra-sensitive gas detection of large-area boron doped graphene, *PNAS*, **2015**, 112, 14527-14532.
10. Lin, Y. C.; Lin, C. Y.; Chiu, P. W. Controllable graphene N-doping with ammonia plasma, *App. Phys. Lett.* 2010, 96, 133110.
11. Wei, D.; Liu, Y.; Wang, Y.; Zhang, H.; Huang, L.; Yu, G. Synthesis of N-doped graphene by CVD and its electrical properties, *Nano Lett.* **2009**, 9, 1752
12. Lv, R.; Botello-Mendez, A. R.; Hayashi, T.; Wang, B.; Berkdemir, A.; Hao, Q.; Elias, A. L.; Cruz-Silva, R.; Gutierrez, H. R.; Kim, Y. A.; Muramatsu, H.; Terrones, H.; Charlier, J. V.; Terrones, M. Nitrogen doped graphene, beyond single substitution and enhanced molecular sensing, *Sci. Rep.* **2012**, 2, 586.
13. Lin, Y. C.; Teng, P. Y.; Yeh, C. H.; Koshino, M.; Chiu, P. W.; Suenaga, K. Structural and Chemical dynamics of pyridinic nitrogen defects in graphene, *Nano Lett.* **2015**, 15, 7408-7413.
14. Sharifi, T; Hu, G; Jia, X; Wagberg, T. Formation of active sites for oxygen reduction reactions by transformation of nitrogen functionalities in nitrogen-doped carbon nanotubes, *ACS Nano* **2012**, 6, 8904-8912.
15. Rinzler, A.G.; Liu, J.; Dai, H.; Nikolaev, P.; Huffman, C.B.; Rodriguez-Macias, F.J.; Boul, P.J.; Lu, A.H.; Heymann, D.; Colber, D.T.; *et al.* Large-scale purification of single-wall carbon nanotubes: process, product, and characterization. *Appl. Phys. A* **1998**, 67, 29-37.
16. Chen, Z.; Santoso, I.; Wang, R.; Xie, L.F.; Mao, H.Y.; Huang, H.; Wang, Y.Z.; Gao, X.Y.; Chen, Z.K.; Ma, D.; Wee, A.T.S.; Chen, W. Surface transfer hole doping of epitaxial graphene using MoO₃ thin film. *Appl. Phys. Lett.* **2010**, 96, 213104.
17. Meyer, J.; Kidambi, P. R.; Bayer, B. C.; Weijtens, C.; Kahn, A.; Centeno, A.; Pasquera, A.; Zurutuza, Z.; Robertson, J.; Hofmann, S. Metal oxide induced charge transfer doping and band alignment of graphene electrodes for efficient organic light emitting diodes, *Sci Rep.* **2014**, 4 5380.

18. Sanders, S.; Cabrero-Vilatela, A.; Kidambi, P. R.; Alexander-Webber, J. R.; Weijtens, C.; Braeuninger-Weimer, P.; Aria, A. L.; Oasim, M.; Wilkinson, T. D.; Robertson, J.; Hofmann, S.; Meyer, J.; Engineering high charge transfer n-doping of graphene electrodes and its application to organic electronics, *Nanoscale*, **2015**, 7, 13135-13142.
19. D'Arsie, L.; Esconjauregui, S.; Weatherup, R. S.; Wu, X.U.; Arter, W. E.; Sugime, H.; Cepek, C.; Robertson, J.; Stable, efficient, p-type doping of graphene by nitric acid, *RSC Advances*, **2016**, 6, 113185-113192.
20. Esconjauregui, S.; D'Arsie, L.; Guo, Y. Z.; Yang, J. W.; Sugime, H.; Caneva, S.; Cepek, C.; Robertson, J. Efficient Transfer Doping of carbon nanotube forests by MoO₃, *ACS Nano*, **2015**, 9, 10422-10430.
21. Hellstrom, S. L.; Vogueritchian, M.; Stoltenberg, R. M.; Irfan, I.; Hammock, M.; Wang, Y. B.; Jia, C. C.; Guo, X. F.; Gao, Y. L.; Bao, Z.; Strong and Stable Doping of Carbon Nanotubes and Graphene by MoO_x for Transparent Electrodes, *Nano Letts.* **2012**, 12, 3574-3580.
22. Kondo, D.; Nakano, H.; Zhou, B.; Akiko, I.; Hayashi, K.; Takahashi, M.; Sato, S.; Yokoyama, N. *Proc IEEE IITC*, **2014**, p189.
23. Detlaff-Weglikowski, U.; Skakalova, V.; Graupner, R.; Jhang, S. H.; Kim, B. H.; Lee, H. J.; Ley, L.; Park, J. W.; Tomanek, D.; Roth, S. Effect of SOCl₂ treatment on electrical and mechanical properties of single-wall carbon nanotube networks, *J. Amer. Chem. Soc.* **2005**, 127, 5125-5131.
24. Dresselhaus, M. S.; Dresselhaus, G. Intercalation compounds of graphite, *Adv. Phys.* **1981**, 30 139.
25. Zhao, W.; Tan, P. H.; Liu, J.; Ferrari, A. C. Intercalation of few-layer graphite flakes with FeCl₃; Raman determination of Fermi level, layer by layer decoupling and stability, *J. Amer. Chem. Soc.* **2011**, 133, 5941-5946.
26. Meyer, J.; Khalandovsky, R.; Görrn, P.; Kahn, A. MoO₃ films spin coated from a nanoparticle suspension for efficient hole injection in organic electronics, *Adv. Mater.* **2011**, 23, 70.
27. Meyer, J.; Hamwi, S.; Kroger, M.; Kowalsky, W.; Reidl, T.; Kahn, A. Transition metal oxides for organic electronics; energetics, device physics, and applications, *Adv. Mater.* **2012**, 24, 5408-5427.
28. Clark, S. J.; Segall, M. D.; Pickard, C. J. First principle methods using CASTEP, *Zeitschrift fur Kryst*, **2005**, 220, 567-570.
29. Grimme, S. Semi empirical GGA-type density functional constructed with long-range dispersion correction, *J. Comput. Chem.* **2006**, 27, 1787-1799.
30. Clark, S. J.; Robertson, J. Screened exchange density functional applied to solids, *Phys. Rev. B*, **2010**, 82, 085208.
31. Hu, T.; Gerber, I. C. Theoretical study of interaction of electron donor and acceptor molecules with graphene, *J. Phys. Chem. C*, **2013**, 117, 2411-2420.
32. Nistor, R.A.; Newns, D.M.; Martyna, G.J. The Role of Chemistry in Graphene Doping for Carbon-Based Electronics. *ACS Nano*, **2011**, 5, 3096-3103.
33. Zhan, D.; Sun, L.; Ni, Z. H.; Liu, L.; Fan, X. F.; Wang, Y.; Yu, T.; Lam, Y. M.; Huang, W.; Shen, Z. X. FeCl₃ based few layer graphene intercalation compounds, single linear dispersion electronic band structure and strong charge transfer doping, *Adv. Funct. Mater.* **2010**, 20, 3504-3509.

34. Song, Y.; Fang, W.; Hsu, A. L.; Kong, J. Iron III chloride doping of CVD graphene, *Nanotechnol*, **2014**, 25 395701.
35. Liu, W.; Wang, J.; Banerjee, K. Characterisation of FeCl₃ intercalation doped CVD few-layer graphene, *IEEE Electron Device Letts*, **2016**, 37 1246-1249.
36. Meng, X.; Tongay, S.; Kang, J.; Chen, Z.; Wu, F.; Li, S. S.; Xia, J. B.; Li, J.; Wu, J. FeCl₃ doping, *Carbon*, **2013**, 57, 507-514.
37. Li, Y; Yue, Q. First-principles study of electronic and magnetic properties of FeCl₃-based graphite intercalation compounds, *Physica B: Condensed Matter*, **2013**, 425, 72-77.